Biochemical and Biophysical Research Communications 391 (2010) 990–994

Contents lists available at ScienceDirect

Biochemical and Biophysical Research Communications

journal homepage: www.elsevier.com/locate/ybbrc

Crystal structure of bacterioferritin from *Rhodobacter sphaeroides*

Ki Hyun Nam [a], Yongbin Xu [b], Shunfu Piao [b], Amit Priyadarshi [a], Eun Hye Lee [a], Hye-Yeon Kim [c], Young Ho Jeon [c], Nam-Chul Ha [b], Kwang Yeon Hwang [a,*]

[a] Division of Biotechnology, College of Life Sciences & Biotechnology, Korea University, Seoul 136-701, Republic of Korea
[b] College of Pharmacy and Research Institute for Drug Development, Pusan National University, Busan 609-735, Republic of Korea
[c] Magnetic Resonance Team, Korea Basic Science Institute, Ochang, Chungbuk 363-883, Republic of Korea

ARTICLE INFO

Article history:
Received 23 November 2009
Available online 5 December 2009

Keywords:
Bacterioferritin
Ferroxidase center
Heme binding
Ferritin family
Crystal structure

ABSTRACT

Iron is essential for the survival of organisms, but either excess or deficient levels of iron induce oxidative stress, thereby causing cell damage. As a result, iron regulation is essential for proper cell growth and proliferation in most organisms. Bacterioferritin is a ferritin-like family protein that contains a heme molecule and a ferroxidase site at the di-iron center. This protein plays a primary role in intracellular iron storage for iron homeostasis, as well as in the maintenance of iron in a soluble and non-toxic form. Although several bacterioferritin structures have been determined, no structural studies have successfully elucidated the molecular function of the heme molecule and the ferroxidase center. Here, we report the crystal structure of bacterioferritin from *Rhodobacter sphaeroides*. This protein exists in a roughly spherical configuration via the assembly of 24 subunits. We describe the oligomeric arrangement, ferroxidase center and heme-binding site based on this structure. The protein contains a single iron-binding configuration in the ferroxidase center, which allows for the release of iron by His130 when the protein is in the intermediate state. The heme molecule in *Rs*Bfr is stabilized by shifting of the *van der Waals* interaction center between the porphyrin of the heme and Trp26. We anticipate that further structural analysis will provide a more complete understanding of the molecular mechanisms of members of the ferritin-like family.

Introduction

Iron is essential for cell growth and proliferation in most organisms. It is involved in a variety of critical processes, including DNA synthesis, photosynthesis and biosynthesis [1]. Both deficient and excess levels of iron can lead to oxidative stress. For example, free iron acts as a catalyst for the formation of oxygen free radicals by the Fenton reaction. In addition, DNA-damaging reactions occur via the reduction of ferric iron to ferrous iron (ferroxidase activity) [2–4]. Therefore, effective regulation of cellular iron concentrations is of obvious importance.

To maintain their iron balance, bacterial organisms have developed efficient systems of iron acquisition (e.g., siderophore-based iron acquisition, metal-type ABC transporters and ferrous iron transport) and storage [1]. The iron storage proteins that play an important role in these balancing systems have been classified into three separate groups: ferritins, bacterioferritins and DNA protection during starvation (DPS) proteins. The subunits of all of these proteins are folded to form a four-helix bundle. Ferritins (24-subunits), bacterioferritins (24-subunits) and DPS proteins (12-subunits) assemble to form a roughly spherical protein shell surrounding a central cavity that acts as an iron storage reservoir [1]. Ferritins and bacterioferritins can accommodate at least 2000–3000 iron atoms per 24-subunit structure, whereas the smaller DPS proteins have a storage capacity of ~500 iron atoms per 12-subunit structure [1]. Ferritin and bacterioferritin both bind iron in the ferroxidase center, whereas DPS proteins bind and oxidize ferrous iron at a completely different site [5]. However, bacterioferritin (Bfr) is distinguished from ferritin by the presence of heme. There are 12 heme molecules per 24-subunit Bfr structure located at each of the 12 twofold interfaces between the subunits. The hemes in Bfr are normally protoporphyrin IX (heme b), although the Bfr of *Desulfovibrio desulfuricans* contains a unique heme, called iron-coproporphyrin III [1,6,7]. The heme molecule in Bfr has been proposed to facilitate electron transfer [8,9]. Many crystal structures belonging to the ferritin-like family have been described, thereby providing architectural information and helping to elucidate the functional mechanism of the family [7,10–16]. Nevertheless, the structural information obtained thus far provides only a speculative insight into the molecular mechanisms of Bfr. As a result, additional studies of the ferritin-like family members have been ongoing in an effort to achieve a better understanding of the mechanisms of these proteins [17–19].

* Corresponding author. Fax: +82 2 923 3229.
E-mail address: chahong@korea.ac.kr (K.Y. Hwang).

0006-291X/$ - see front matter © 2009 Elsevier Inc. All rights reserved.
doi:10.1016/j.bbrc.2009.12.003

Here, we report the crystal structure of the 'as-isolated' bacterioferritin from *Rhodobacter sphaeroides*, which we have named *Rs*Bfr. This protein exists as a highly symmetrical oligomeric spherical structure formed by 24-subunits. The spherical architecture of *Rs*Bfr contains 24 irons of low occupancy in the ferroxidase center and 12 heme molecules. We also describe the configuration of the ferroxidase center and heme-binding site of *Rs*Bfr and provide a comparison of this compound with other bacterioferritins. We anticipate that this structural analysis will broaden our understanding of the molecular functions of the ferritin-like family.

Materials and methods

Purification and crystallization. Crystallization of bacterioferritin from *R. sphaeroides* occurred accidentally while attempting to crystallize cytochrome cbb_3 cytochrome oxidase. *Rhodobacter sphaeroides* cell lysates were subjected to centrifugation at 14,000 rpm for 30 min, and the supernatants were collected and loaded onto a Hi-Trap Q column (GE Healthcare) that had been pre-equilibrated with buffer (20 mM Tris–HCl, pH 8.0 and 200 mM NaCl). The protein was then eluted using a linear NaCl gradient that ranged from 0.2 to 1 M (in 20 mM Tris–HCl, pH 8.0, 200 mM NaCl and 0.02% (w/v) *n*-dodecyl-β-D-maltopyranoside). The eluted protein samples were loaded onto a His Trap column (GE Healthcare) that had been pre-equilibrated with buffer (20 mM Tris–HCl, pH 8.0, 200 mM NaCl and 0.02% (w/v) *n*-dodecyl-β-D-maltopyranoside). The protein was then eluted using a linear imidazole gradient that ranged from 0 to 0.5 M (in 20 mM Tris–HCl, pH 8.0, 200 mM NaCl and 0.02% (w/v) *n*-dodecyl-β-D-maltopyranoside). Finally, we purified the protein using a HiTrap Q column (GE Healthcare) by repeating the first-step purification method. The *Rs*Bfr crystals were formed in 0.1 M Na-citrate, pH 5.6 and 14–20% (w/v) PEG 200 using the hanging drop vapor diffusion method. Suitable crystals for X-ray data collection appeared after 6 months.

Data collection and processing. The *Rs*Bfr crystal was flash frozen in mother liquor containing 25% (v/v) glycerol. Diffraction data were collected at beamline 4A (wavelength 1.000 Å) at the Pohang Light Source (Pohang, Korea). The data were then indexed and integrated with the DENZO and SCALEPACK programs from the HKL2000 program package [20]. The initial phases were obtained by molecular replacement with bacterioferritin from *Rhodobacter captulus* (PDB code: 1JGC). Molecular replacement was performed with MOLREP from the CCP4 suite [21]. The model refinement, initial selection and manual verification of water molecules were conducted using the CNS software suite [22]. The model was adjusted with σ A-weighted $F_o - F_c$ and $2F_o - F_c$ electron density maps using the Coot program [23]. Final refinement was conducted using the Refmac5 program from the CCP4 suite [24]. Final validation of the stereochemical quality of the final model was assessed using MolProbity [25]. The illustrations of the crystal structure were prepared with PyMOL (www.pymol.org). The data collection and structure refinement statistics are shown in Table 1.

Accession code. The final coordinates and structural factors of bacterioferritin from *R. sphaeroides* have been deposited into the Protein Data Bank under the accession codes 3GVY.

Table 1
Data collection and refinement statistics of bacteroferritin.

Data collection	
Space group	*I*422
Cell parameter (Å)	$a = b = 160.495$, $c = 116.276$
Resolution (Å)	50–2.80 (2.90–2.80)
Completeness	89.4 (81.4)
Redundancy	5.2 (2.9)
$I/\sigma(I)$	8.71 (2.74)
R_{merge}[a] (%)	0.142 (0.357)
Refinement statistics	
Resolution	41.57–2.80
R_{work}/R_{free}[b] (%)	22.9/28.5
Averaged *B*-factor (Å^2)	
Protein	35.28
Heme	55.48
Metal (Iron)	61.26
rms deviations	
Bond lengths (Å)	0.019
Bond angles (°)	1.758
Ramachandran plot (%)	
Favored	93.1
Allowed	6.7
Disallowed	0.2

The highest-resolution shell is shown in parentheses.

[a] $R_{merge} = \sum_h \sum_i |I(h,ii) - \langle I(h)\rangle| / \sum_h \sum_i I(h,ii)$, where $I(h,i)$ is the intensity of the *i*th measurement of reflection *h* and $\langle I(h)\rangle$ is the mean value of $I(h,i)$ for all *i* measurements.

[b] $R_{work} = \sum||F_{obs}| - |F_{calc}|| / \sum|F_{obs}|$, where F_{obs} and F_{calc} are the observed and calculated structure-factor amplitudes, respectively. R_{free} was calculated as R_{work} using a randomly selected subset (5.1%) of unique reflections not used for structural refinement.

Results and discussion

Structural analysis of bacterioferritin from R. sphaeroides

The space group of the crystal structure of *Rs*Bfr was determined to be the tetragonal *I*422 space group, with unit cell dimensions of $a = b = 160.49$ Å and $c = 116.27$ Å, with three subunits occupying the asymmetric unit (Fig. 1A). The crystal structure of *Rs*Bfr was determined at 2.80 Å, at which nearly the entire electron density map showed clear density (Met1-Asp158, except for three C-terminal residues). The *Rs*Bfr subunit is composed primarily of α-helical secondary structure (~80%), with an α-helix bundle (α1–α4), a tilted α-helix at the C-terminal (α5) and a long loop between the α-helices 2 and 3. The average rms deviation obtained when the three *Rs*Bfr subunits of the asymmetric unit were superimposed on their Cαs (Ala-5-Asn153) was 0.32 Å. The *Rs*Bfr protein forms an oligomeric structure composed of 24 subunits with a roughly spherical architecture of approximately $110 \times 110 \times 110$ Å and 1330 nm^3 (Fig. 1B). Each subunit is almost completely buried by the five neighboring subunits. The spherical *Rs*Bfr configuration has an external diameter of approximately 110 Å and an internal cavity with a diameter of approximately 80 Å. Dimer formation in the *Rs*Bfr structure is believed to follow the basic assembly procedure (subunit I and II in Fig. 1A) that is common among other members of the ferritin family [7,10–16]. Based on this dimer formation, the subunit in the spherical architecture has a 432 point group symmetry that forms a cube. This cube consists of six fourfold axes, eight threefold axes and two twofold axes. The fourfold and threefold axes form a narrow channel that is believed to be the iron entrance pore [7,10–16].

The ferroxidase center is located within the four α-helix bundle of each subunit (Fig. 1C). The ferroxidase center catalyzes the oxidation of ferrous iron to ferric iron and is responsible for the ferroxidase activity of Bfr [12,13]. In the interior of the four-helix bundle of *Rs*Bfr, electron density at the first iron binding site (denoted Fe1) was clearly observed, whereas electron density at the second iron binding site (denoted Fe2) was not observed (Fig. 1C). Although the iron at the Fe1 site has a temperature factor approximately twofold (approximately 60 Å^2) higher than the average temperature factor of *Rs*Bfr (approximately 35 Å^2), it is stabilized by tetrahedral coordination with Glu18, Glu51, His54 and Glu127. Based on this structure, the Oε atoms of Glu18, Glu51 and Glu127 exist in a delocalized state as carboxylates and interact with the iron at the Fe1 site at distances of approximately ~2.4 Å. The Nδ atom of His54 associates with iron at the Fe1 site at a distance of approximately 2.5 Å. Interestingly, the Nε atom of His54 forms a salt bridge with the Oδ atom of Asp126 at a

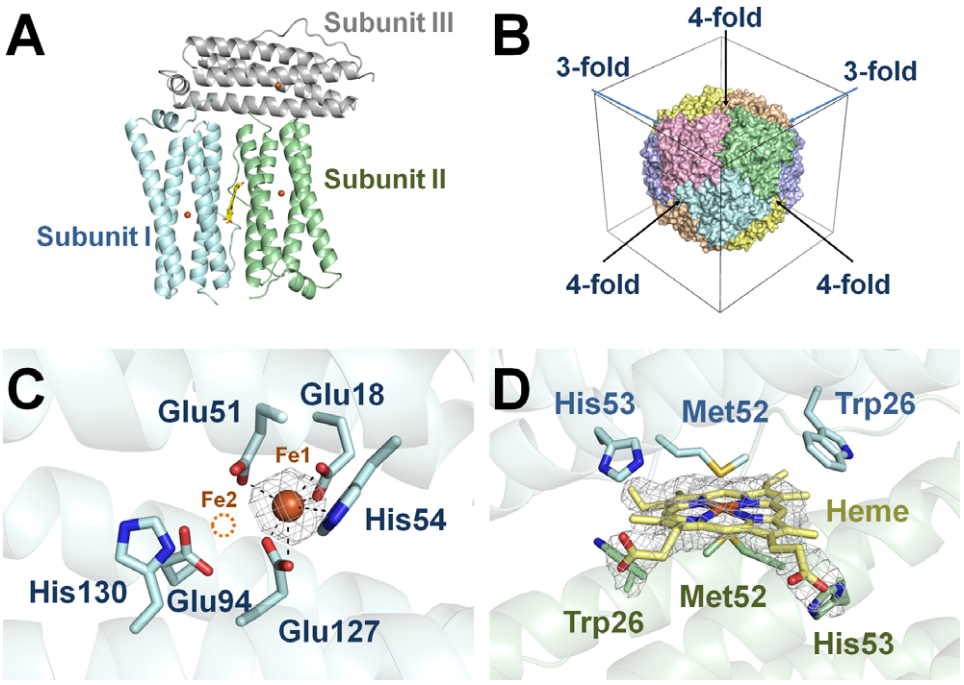

Fig. 1. Crystal structure of *Rs*Bfr. (A) Three *Rs*Bfr subunits contained in an asymmetric unit with an *I*422 space group. The heme molecule is located at the center of the interface between subunit I and subunit II. Each subunit contains an iron molecule that is encompassed by the helix bundle. (B) The *Rs*Bfr architecture has an external diameter of approximately 110 Å that is formed by the assembly of 24 subunits. Each color indicates a pair of subunits. The architecture of the cubic center has 432 point group symmetry. In addition, the subunit consists of 6 fourfold axes, 8 threefold axes and 2 twofold axes. The fourfold and threefold axes comprise the iron entrance pore. (C) The ferroxidase center of *Rs*Bfr. In the interior of the four-helix bundle of *Rs*Bfr, the iron at the Fe1 site was easily observed in the $2F_o - F_c$ electron density map (contoured at 2.0σ). The Fe2 site is indicated by the dashed orange circle. The iron at the Fe1 site is tetrahedrally coordinated by Glu18, Glu51, His54 and Glu127. Two Oε atoms in three glutamate residues (Glu18, Glu51 and Glu127) exist in a delocalized carboxylate state. (D) The heme-binding site in *Rs*Bfr. The heme molecule is located at the twofold symmetry center between two *Rs*Bfr subunits. The $2F_o - F_c$ electron density map (contoured at 2.0σ) is shown in gray. Trp26, Met52 and His53 interact with the heme molecule. The His53 residue and the oxygen atom of the heme form a salt bridge. The interaction between Trp26 and the heme is stabilized by a *van der Waals* interaction. The sulfur atom of Met52 is near the iron center of the heme molecule and forms a bis-methionine ligation to the heme molecule.

distance of approximately 3.5 Å. Taken together, these characteristics demonstrate that the iron at the Fe1 site in *Rs*Bfr is stabilized by the conjugated base of the glutamic acids and strictly positioned in relation to the histidine residue. In previously reported Bfr structures, iron bound at the Fe2 site was observed near the Fe1 site at a distance of approximately 3.5 Å [10]. However, the bound iron at the Fe2 site generally had a low occupancy and a weak position in the $F_o - F_c$ electron density map [12]. It appears that various iron configurations exist in Bfr structures, a finding that adds new dimension to the understanding of the architectural mechanisms of Bfr.

In the crystal structure of *Rs*Bfr, heme molecules are located on the twofold symmetric subunit interface (Fig. 1D). The heme molecule had temperature factors that were approximately 50% twofold (approximately 55.5 $Å^2$, with the exception of the propionate group) higher than the average temperature factors of *Rs*Bfr (approximately 35 $Å^2$), indicating that the two subunits of *Rs*Bfr are held loosely in the pocket. When the electron density was evaluated, the porphyrin and iron-center were well defined, but the vinyl and propionate groups showed only weak electron density. The vinyl group of the heme is buried in the interface between each subunit of dimer formation, and the propionate group is exposed to the internal cavity. Although the heme molecule of *Rc*Bfr has been reported to have two orientations [12], we did not clearly observe separate orientations of the heme molecule in *Rs*Bfr. The *Rs*Bfr heme molecule interacts with two residues of Met52 and His53 within the distance cutoff of 3.2 Å. Additionally, the C5 atoms of Trp26 interact with the porphyrin of the heme molecule at 3.5 Å, which indicates that the Trp26 residue contributes to stabilization of the heme molecule via the *van der Waals* interaction. Conversely, the Nε atom of His53 and the propionate group of the heme molecule form a salt bridge of approximately 3.4 Å; however, although this interaction is considered to be close, we believe it is also weak, based on the low occupancy of the carboxyl group in the electron density map. The sulfur atom of Met52 encloses the iron-center in the heme, which results in a hydrophobic interaction. In general, the heme molecule is stabilized by cysteine or histidine residues, but the iron-center in the heme molecule of *Rs*Bfr is stabilized by the Sε atom of Met52, a configuration that is shared by other bacterioferritins [7,10–16]. In the *Rs*Bfr structure, the heme molecule is stabilized by three residues (Trp26, Met52 and His53) as well as by several other hydrophobic residues. The interface between subunits I and II results in the formation of a hydrophobic cavity by Leu19, Val22, Ser23, Trp26, Arg45, Ile49, Met52, His53 and Ala55. In addition, approximately 70% (~700 $Å^2$) of the heme molecule is buried by the surfaces of subunits I and II. Taken together, the architectural characteristics of *Rs*Bfr indicate that the heme molecule in *Rs*Bfr is stabilized by several hydrophobic interactions.

Comparison with other bacterioferritins

We compared the structure of the bacterioferritin described here with those of *Rc*Bfr (from *Rhodobacter capsulatus*), *Ec*Bfr (from *Escherichia coli*) and *Av*Bfr (from *Azotobacter vinelandii*) to explore the structural differentiation of these molecules. The *Rs*Bfr protein shared amino acid sequence identities of 67.7%, 48.3% and 49.0% with *Rc*Bfr, *Ec*Bfr and *Av*Bfr, respectively (Fig. 2A). All of the structures had a spherical architecture similar to that of ferritin, with 24 subunits and 432 point group symmetry. The superimposition of the atomic coordinates of the *Rs*Bfr subunit and its dimers with

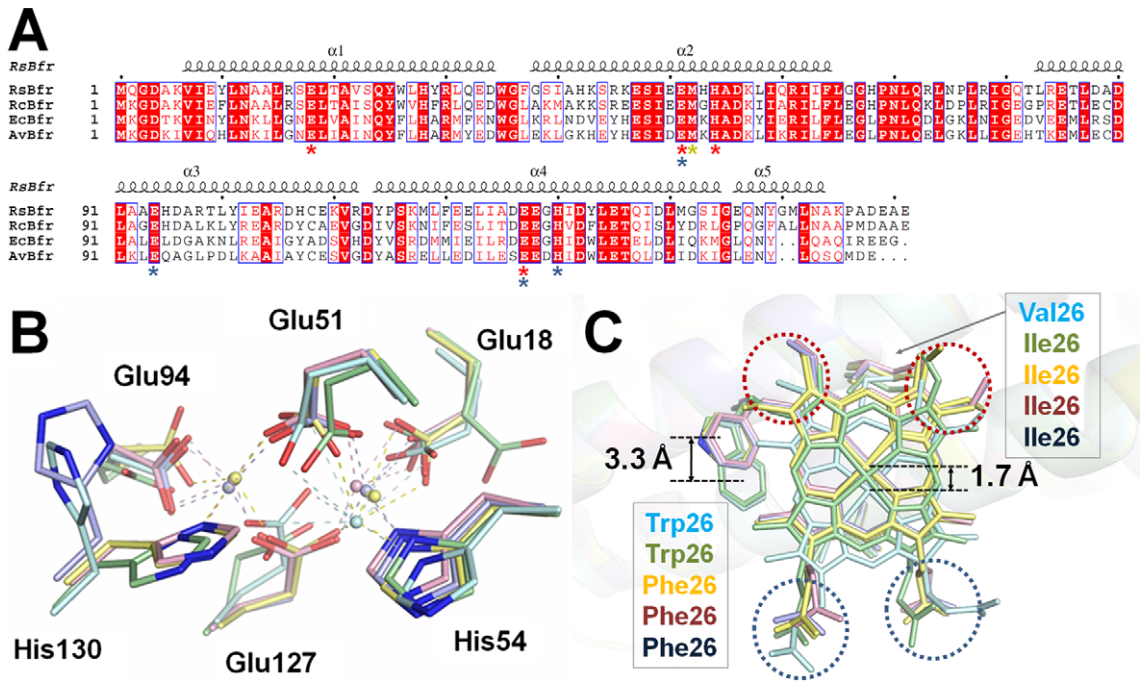

Fig. 2. Sequential and structural comparison with other Bfr proteins. (A) Multiple sequence alignment of *Rs*Bfr (Accession No. Q3J696) with *Rc*Bfr (Q59738), *Ec*Bfr (P0ABD3) and *Av*Bfr (P22759) was performed with ClustalW2. Conserved amino acids in the Bfrs are shown in red. The secondary structure of *Rs*Bfr is indicated by a black coil for α-helices and empty space for loops. The iron coordination residues (Glu18, Glu51, His54 and Glu127) at the Fe1 site are indicated by red asterisks. The iron interaction residues (Glu51, Glu94, Glu127 and His130) at the Fe2 site are indicated by blue asterisks. The heme axial ligand, Met52, is indicated by yellow asterisks. (B) Superimposition of the ferroxidase center of the Bfr structures. *Rs*Bfr, *Rc*Bfr, *Ec*Bfr, *Av*Bfr (oxidized) and *Av*Bfr (reduced) are indicated by cyan, green, yellow, pink and blue, respectively. *Ec*Bfr and *Av*Bfr are shown in the di-iron-binding configuration. Among these structures, *Av*Bfr has a different orientation at His130 in the reduced state. *Rs*Bfr contains an iron at the Fe1 site, and the His130 residue of the *Rs*Bfr structure is enclosed in the *Av*Bfr structure in the reduced state. (C) Superimposition of the heme-binding site of the Bfr structures. Heme molecules in the Bfr structures are commonly coordinated by methionine residues. The propionate region (blue dot-circles) in the heme molecules lacks a rigid conformation and exposes the internal cavity. The vinyl group (red dot-circles) in the heme molecule has two orientations and configurations. The heme ligation methionine residue of *Rs*Bfr is shifted towards the internal cavity. Three hydrophobic residues (Val22, Ile49 and Met52 in *Rs*Bfr) showed similar shifts. A structural comparison of *Rs*Bfr and *Ec*Bfr shows that the *van der Waals* force center also shifts. *Rs*Bfr, *Rc*Bfr, *Ec*Bfr, *Av*Bfr (oxidized) and *Av*Bfr (reduced) are indicated by cyan, green, yellow, pink and blue sticks in the illustration, respectively.

those of *Rc*Bfr (PDB code: 1JGC), *Ec*Bfr (2HTN) and *Av*Bfr (2FL0; oxidized and 2FKZ; reduced) resulted in Cα rms deviations of 0.34, 0.67 and 0.64 Å, respectively. When a structural comparison of the architecture was conducted, all of the Bfr structures commonly shared the three- and fourfold architecture. These symmetric pores of the Bfr structures suggested that there was an ion channel at the three- and fourfold axes that functions in ferrous conductivity and selectivity [7,10–16]. However, the ion interaction residues displayed different amino acid sequences and exhibited different structural formation than the superimposed structure. In addition, although the *Rs*Bfr, *Av*Bfr and *Ec*Bfr structures shared several common residues (Asn in the fourfold axes and Glu in the threefold axes) and appeared to possess iron selectivity, *Rc*Bfr contained different residues, which were primarily hydrophobic, at the same coordination point. Although selectivity of the symmetric iron pores was observed in several Bfr structures, the pores played different molecular roles depending on the organism from which they were obtained. Therefore, further studies to acquire additional structural and biological information regarding these iron pores are necessary. Conversely, comparison of the amino acid structures revealed that the ferroxidase sites (Glu18, Glu51, His54, Glu94, Glu127 and His130 in *Rs*Bfr) and heme-binding residues (Met52 in *Rs*Bfr) were strictly conserved, and that these residues had similar structural properties. Based on the reported structure, Glu51, Glu94, Glu127 and His130 (in *Rs*Bfr numbering) interact with the iron at Fe2, thereby forming a tetrahedral coordination (Fig. 2B). However, the two Oε atoms of Glu51 and Glu127 in *Rs*Bfr structure interact with the iron at Fe1, and the Oε atom of Glu94 partially interacts with the Oε atom of Glu127. Conversely, the side chain of His130 in *Rs*Bfr structure has a different orientation from that of the side chain of His130 from other structures based on comparison with the ferroxidase site in the Bfr structure. In general, two irons bind in the ferroxidase center located in the interior of the four-helix bundle, which prevents their release. However, the crystallized *Rs*Bfr structure is in the released conformation at the Fe2 position, a conformation that we consider to be in the intermediate state. When the heme-binding site of the Bfr structure was evaluated, a common hydrophobic pocket was found to exist within the twofold symmetric dimer between the two subunits. Additionally, conserved methionine residues interact with the iron-center in the heme molecule, resulting in the ligation of bis-methionine to the heme molecule [26,27]. However, evaluation of the superimposed structures revealed that the heme molecule in the *Rs*Bfr and *Rc*Bfr structures shifted towards the internal space by approximately 1.7 Å (Fig. 2C). Examination of the structures revealed the reason for the shifting of the heme molecule. Specifically, *Bc*Bfr and *Av*Bfr contain a phenylalanine residue in the hydrophobic pocket between the twofold symmetric dimers, which results in a *van der Waals* interaction with porphyrin. However, in *Rs*Bfr and *Rc*Bfr, tryptophan residues are located at that position in the hydrophobic pocket. Thus, the heme molecules in *Rs*Bfr and *Rc*Bfr are stabilized by shifting of the *van der Waals* interaction center between porphyrin and Trp26. Furthermore, *Rs*Bfr and *Rc*Bfr also contain different coordination positions; the heme shift is affected by the differences in the hydrophobic residues in the pocket. Nevertheless, the entire heme molecule is coordinated by methionine into the bis-methionine ligation. As a result, the heme molecule has a different atomic interaction that is affected by component residues

in the hydrophobic pocket between the twofold symmetric dimers, but its molecular coordination is similar, including the ligation of methionine and interactions with the hydrophobic interface.

In summary, we report the crystal structure of 'as-isolated' bacterioferritin from *R. sphaeroides*. The crystal structure of *Rs*Bfr reveals a unique configuration in the ferroxidase center and heme-binding site. We believe that this information is a significant contribution to our understanding of and insight into the molecular mechanisms of bacterioferritins.

Acknowledgments

We thank the staff for their assistance during the data collection at Beamline 4A of the Pohang Light Source, Korea. This study was supported by the Functional Proteomics Center, 21C Frontier Program, of the Korea Ministry of Science and Technology and the K-MeP of Korea Basic Science Institute. K.H. Nam was supported by a Research Fellowship from the BK21 Project.

References

[1] S.C. Andrews, A.K. Robinson, F. Rodriguez-Quinones, Bacterial iron homeostasis, FEMS Microbiol. Rev. 27 (2003) 215–237.
[2] P.B. Walter, M.D. Knutson, A. Paler-Martinez, S. Lee, Y. Xu, F.E. Viteri, B.N. Ames, Iron deficiency and iron excess damage mitochondria and mitochondrial DNA in rats, Proc. Natl. Acad. Sci. USA 99 (2002) 2264–2269.
[3] K. Orino, L. Lehman, Y. Tsuji, H. Ayaki, S.V. Torti, F.M. Torti, Ferritin and the response to oxidative stress, Biochem. J. 357 (2001) 241–247.
[4] S. Linn, DNA damage by iron and hydrogen peroxide in vitro and in vivo, Drug Metab. Rev. 30 (1998) 313–326.
[5] A. Ilari, S. Stefanini, E. Chiancone, D. Tsernoglou, The dodecameric ferritin from *Listeria innocua* contains a novel intersubunit iron-binding site, Nat. Struct. Biol. 7 (2000) 38–43.
[6] C.V. Romao, R. Louro, R. Timkovich, M. Lubben, M.Y. Liu, J. LeGall, A.V. Xavier, M. Teixeira, Iron-coproporphyrin III is a natural cofactor in bacterioferritin from the anaerobic bacterium *Desulfovibrio desulfuricans*, FEBS Lett. 480 (2000) 213–216.
[7] S. Macedo, C.V. Romao, E. Mitchell, P.M. Matias, M.Y. Liu, A.V. Xavier, J. LeGall, M. Teixeira, P. Lindley, M.A. Carrondo, The nature of the di-iron site in the bacterioferritin from *Desulfovibrio desulfuricans*, Nat. Struct. Biol. 10 (2003) 285–290.
[8] B. Zhang, J.N. Harb, R.C. Davis, S. Choi, J.W. Kim, T. Miller, S.H. Chu, G.D. Watt, Electron exchange between Fe(II)-horse spleen ferritin and Co(III)/Mn(III) reconstituted horse spleen and *Azotobacter vinelandii* ferritins, Biochemistry 45 (2006) 5766–5774.
[9] G.D. Watt, R.B. Frankel, G.C. Papaefthymiou, K. Spartalian, E.I. Stiefel, Redox properties and Mossbauer-spectroscopy of *Azotobacter vinelandii* bacterioferritin, Biochemistry 25 (1986) 4330–4336.
[10] F. Frolow, A.J. Kalb, J. Yariv, Structure of a unique twofold symmetric haem-binding site, Nat. Struct. Biol. 1 (1994) 453–460.
[11] A. Dautant, J.B. Meyer, J. Yariv, G. Precigoux, R.M. Sweet, A.J. Kalb, F. Frolow, Structure of a monoclinic crystal from of cytochrome *b*1 (Bacterioferritin) from *E. coli*, Acta Crystallogr. D Biol. Crystallogr. 54 (1998) 16–24.
[12] D. Cobessi, L.S. Huang, M. Ban, N.G. Pon, F. Daldal, E.A. Berry, The 2.6 Å resolution structure of *Rhodobacter capsulatus* bacterioferritin with metal-free dinuclear site and heme iron in a crystallographic 'special position', Acta Crystallogr. D Biol. Crystallogr. 58 (2002) 29–38.
[13] H.L. Liu, H.N. Zhou, W.M. Xing, J.F. Zhao, S.X. Li, J.F. Huang, R.C. Bi, 2.6 Å resolution crystal structure of the bacterioferritin from *Azotobacter vinelandii*, FEBS Lett. 573 (2004) 93–98.
[14] L. Swartz, M. Kuchinskas, H. Li, T.L. Poulos, W.N. Lanzilotta, Redox-dependent structural changes in the *Azotobacter vinelandii* bacterioferritin: new insights into the ferroxidase and iron transport mechanism, Biochemistry 45 (2006) 4421–4428.
[15] R. Janowski, T. Auerbach-Nevo, M.S. Weiss, Bacterioferritin from *Mycobacterium smegmatis* contains zinc in its di-nuclear site, Protein Sci. 17 (2008) 1138–1150.
[16] S.C. Willies, M.N. Isupov, E.F. Garman, J.A. Littlechild, The binding of haem and zinc in the 1.9 Å X-ray structure of *Escherichia coli* bacterioferritin, J. Biol. Inorg. Chem. 14 (2009) 201–207.
[17] S. Abe, J. Niemeyer, M. Abe, Y. Takezawa, T. Ueno, T. Hikage, G. Erker, Y. Watanabe, Control of the coordination structure of organometallic palladium complexes in an apo-ferritin cage, J. Am. Chem. Soc. 130 (2008) 10512–10514.
[18] M. Sutter, D. Boehringer, S. Gutmann, S. Guenther, D. Prangishvili, M.J. Loessner, K.O. Stetter, E. Weber-Ban, N. Ban, Structural basis of enzyme encapsulation into a bacterial nanocompartment, Nat. Struct. Mol. Biol. 15 (2008) 939–947.
[19] A. Marchetti, M.S. Parker, L.P. Moccia, E.O. Lin, A.L. Arrieta, F. Ribalet, M.E.P. Murphy, M.T. Maldonado, E.V. Armbrust, Ferritin is used for iron storage in bloom-forming marine pennate diatoms, Nature 457 (2009) 467–470.
[20] Z. Otwinowski, W. Minor, Processing of X-ray diffraction data collected in oscillation mode, Macromol. Crystallogr. A 276 (1997) 307–326.
[21] A. Vagin, A. Teplyakov, MOLREP: an automated program for molecular replacement, J. Appl. Crystallogr. 30 (1997) 1022–1025.
[22] A.T. Brunger, P.D. Adams, G.M. Clore, W.L. DeLano, P. Gros, R.W. Grosse-Kunstleve, J.S. Jiang, J. Kuszewski, M. Nilges, N.S. Pannu, R.J. Read, L.M. Rice, T. Simonson, G.L. Warren, Crystallography & NMR system: a new software suite for macromolecular structure determination, Acta Crystallogr. D Biol. Crystallogr. 54 (1998) 905–921.
[23] P. Emsley, K. Cowtan, Coot: model-building tools for molecular graphics, Acta Crystallogr. D Biol. Crystallogr. 60 (2004) 2126–2132.
[24] M.D. Winn, G.N. Murshudov, M.Z. Papiz, Macromolecular TLS refinement in REFMAC at moderate resolutions, Methods Enzymol. 374 (2003) 300–321.
[25] I.W. Davis, A. Leaver-Fay, V.B. Chen, J.N. Block, G.J. Kapral, X. Wang, L.W. Murray, W.B. Arendall 3rd, J. Snoeyink, J.S. Richardson, D.C. Richardson, MolProbity: all-atom contacts and structure validation for proteins and nucleic acids, Nucleic Acids Res. 35 (2007) W375–W383.
[26] M.R. Cheesman, F.H. Kadir, J. al-Basseet, F. al-Massad, J. Farrar, C. Greenwood, A.J. Thomson, G.R. Moore, E.p.r. and magnetic circular dichroism spectroscopic characterization of bacterioferritin from *Pseudomonas aeruginosa* and *Azotobacter vinelandii*, Biochem. J. 286 (Pt 2) (1992) 361–367.
[27] P. Nordlund, H. Eklund, Di-iron-carboxylate proteins, Curr. Opin. Struct. Biol. 5 (1995) 758–766.